

Delayed interactions in the noisy voter model through the periodic polling mechanism

Aleksejus Kononovicius^{1*}, Rokas Astrauskas², Marijus Radavičius³, Feliksas Ivanauskas²

¹ - Institute of Theoretical Physics and Astronomy, Vilnius University

² - Institute of Computer Science, Vilnius University

³ - Institute of Applied Mathematics, Vilnius University

Abstract

We investigate the effects of delayed interactions on the stationary distribution of the noisy voter model. We assume that the delayed interactions occur through the periodic polling mechanism and replace the original instantaneous two-agent interactions. In our analysis, we require that the polling period aligns with the delay in announcing poll outcomes. As expected, when the polling period is relatively short, the model with delayed interactions is almost equivalent to the original model. As the polling period increases, oscillatory behavior emerges, but the model with delayed interactions still converges to stationary distribution. The stationary distribution resembles a Beta-binomial distribution, with its shape parameters scaling with the polling period. The observed scaling behavior is non-monotonic. Namely, the shape parameters peak at some intermediate polling period.

1 Introduction

In the physics realm, interactions among spatially distributed elements are subject to temporal delay, as any physical interaction is inherently bound by a finite propagation speed. Similarly, within the biological sphere, communication between biological entities relies on biochemical materials that also move at finite speeds [1–3]. Everyday social dynamics are equally affected by propagation constraints arising from limited information processing capacities and finite learning speeds [4–7]. The finite speed of information propagation across diverse systems results in temporal delays, giving rise to intricate phenomena. These delays manifest in phenomena such as stabilization of chaotic systems [8–11], resonant behavior in stochastic systems [12–14], and pattern formation in evolutionary game dynamics and social systems [15–18], among others. In real-world scenarios, public opinion polls often take significant time to be conducted, processed, and subsequently released to the public. Consequently, the polling mechanism can be seen as a source of delays in the opinion formation process. Here, we focus on the implications of information delays induced by the periodic polling mechanism on the opinion formation process.

Modeling opinion formation is a primary concern within an emerging subfield of statistical physics known as sociophysics [19–25]. Opinion formation models describe the evolution of opinions within artificially simulated societies as if they were describing magnetization phenomena in spin systems. The voter model [26, 27] stands out as one of the most thoroughly examined models in the field of sociophysics. Introduced as a model for spatial conflict between competing species, it has gained substantial popularity in opinion dynamics and, for this reason, is known as the voter model [20]. In the context of opinion dynamics, the spatial dimension from the original model is replaced by a social network of individuals. Likewise, the competing species from the original model are replaced by competing opinions that the individuals could possess. From the statistical

*corresponding author; email: aleksejus.kononovicius@tfai.vu.lt; website: kononovicius.lt.

physics perspective, we could interpret an individual as a kind of social particle (referred as agents) and the distinct opinions as the available states for the particles to be in. While multi-state generalizations of the model exist [28–30], most of the literature focuses on the other possible generalizations of the voter model retaining the binary opinions [22–24].

Here, we are particularly interested in a generalization known as the noisy voter model [31]. An analogous model was introduced earlier in [32], hence this generalization is occasionally referred to as Kirman’s herding model. Both of these approaches extend the voter model by allowing independent single-agent transitions. In contrast to the voter model, the noisy voter model doesn’t converge to a fixed state (either full or partial consensus); instead, it converges in a statistical sense to a broad stationary distribution. Stationary distribution of the noisy voter model is known to fit political party vote share distributions across various elections quite well [33–36]. Therefore, it can be seen as a minimal model for the political opinion formation in the society. Consequently, the noisy voter model appears to be a natural choice to explore the implications of information delays induced by the periodic polling mechanism.

Latency in binary opinion formation processes, including the voter model, was earlier considered in [37]. Contrary to our approach to temporal delays, Lambiotte et al. have considered latency from an individual agent perspective. Namely, it was assumed that individual agents become inactive immediately after changing their state, but they may become activated again after some time. In the latent opinion formation process, the inactive agents are effectively equivalent to zealots, as they are unable to change their state, but they may influence other agents. Later works have built upon the ideas of the latent opinion formation process or from similar considerations arrived at their independent approaches, but many of them working towards studying physics-inspired aging and other state freezing effects [38–41]. In our approach, latency creates an effect similar to zealotry [42–46], but with the difference that agents change their state without other agents perceiving these changes until the announcement of the poll outcome. Simulating polls was also addressed in a few earlier works [46, 47], but these approaches were more data-centric and therefore have not considered possible latency effects or periodic driving of the electoral system.

This paper is structured as follows. In Section 2, we briefly discuss the original noisy voter model and then generalize it by introducing the periodic polling mechanism. Having defined the microscopic behavior rules, we introduce three distinct simulation methods tailored for the generalized model with period polling, see Section 3. In Section 4 we explore the stationary poll outcome distributions both analytically and numerically. In the short polling period limit, the delay has a negligible effect. In the long polling period limit, the stationary distribution of the generalized model is well approximated by the Beta-binomial distribution with the shape parameters twice as large as the independent transition rates. This finding suggests that the periodic polling mechanism decreases the variance of the poll outcome distribution. Yet the maximum of this effect is observed for some intermediate polling period. Based on the approximation by a second order auto-regressive process [48], we are able to derive explicit analytical form of the scaling law as well as the location of its maximum. In Section 5, we analyze periodic fluctuations induced by the periodic polling mechanism. While the scaling behavior of the power spectral density follows a trivial monotonic sigmoid-like functions, some interesting behavior is recovered by examining the variance of the consecutive and the next-consecutive poll swings. Finally, all findings are briefly summarized and future outlook is given in Section 6.

2 Definition of the noisy voter model with the periodic polling mechanism

The noisy voter model describes the dynamics of a fixed number of agents, denoted as N , switching between two possible states labeled as “0” and “1”. Agents switch their states independently at a rate σ_i , where i represents the label of the destination state, or they imitate the states of their peers at a rate h . Since only one agent changes its state at any given time, we can express the system-wide transition rates with respect to the number

of agents in state “1”, denoted by X , as follows:

$$\lambda(X \rightarrow X + 1) = \lambda^+ = (N - X) [\sigma_1 + hX], \quad \lambda(X \rightarrow X - 1) = \lambda^- = X [\sigma_0 + h(N - X)]. \quad (1)$$

Since the transition rates remain constant between the updates of the system state X , simulating this model follows a standard approach similar to any other homogeneous Poisson process. For example, this model could be simulated by using one-step transition probability approach [49], or by using Gillespie method [50].

In the $N \rightarrow \infty$ limit it is trivial to show that $x = \frac{X}{N}$ is distributed according to the Beta distribution, $x \sim \mathcal{Be}(\frac{\sigma_1}{h}, \frac{\sigma_0}{h})$. For the finite N , X would be distributed according to the Beta-binomial distribution, $X \sim \text{BetaBin}(N, \frac{\sigma_1}{h}, \frac{\sigma_0}{h})$. As the shape parameters of the stationary distribution depend only on the ratio of σ_i and h , we can simplify the model by introducing dimensionless parameters $\varepsilon_i = \frac{\sigma_i}{h}$ and simulate the model in dimensionless time $t = ht'$ (here t' is the physical time measured in desired time units).

Let us generalize the noisy voter model by restricting imitative interactions to occur solely through the periodic polls. We denote the polling period as τ . Let us assume that the polls perfectly reflect the system state at the time of polling, but their outcomes are announced with a delay. To keep the model simple, we assume that this delay coincides with the polling period. Under these assumptions, the system-wide transition rates become:

$$\lambda_k^+ = (N - X) [\varepsilon_1 + A_{k-1}], \quad \lambda_k^- = X [\varepsilon_0 + (N - A_{k-1})], \quad (2)$$

where $k = \lfloor \frac{t}{\tau} \rfloor$ is the index of the last conducted poll, and A_{k-1} is the last announced poll outcome. In general k -th poll outcome would be defined as

$$A_k = X \left(\left\lfloor \frac{t}{\tau} \right\rfloor \tau \right). \quad (3)$$

As implied by the form of the rates (2), at time t , the most recently conducted poll outcome A_k has not yet been announced. Instead, the agents are aware of the outcome of an earlier poll A_{k-1} , which we refer to as the last announced poll outcome. For example, at $t = 0$ the outcome A_{-1} is announced (it must be specified as a part of the initial condition), and the outcome A_0 is recorded. Effectively it is also given as a part of the initial condition, as $A_0 = X(0)$. The outcome of initial poll A_0 will be announced at $t = \tau$. Fig. 1 depicts a sample time series generated by the model, extending up to $t = 5\tau$. The red curve traces the evolution of the system state, $X(t)$, while the black curves depict the last announced poll outcome A_{k-1} (solid curve) and the last conducted poll outcome A_k (dotted curve). At the start of each polling period, at $t = k\tau$, the dotted curve intersects both the solid curve and the red curve. As information about the last conducted poll is made known, the solid curve catches up to the dotted curve. Immediately afterwards, a new poll is conducted, which is represented by the dotted curve catching up to the red curve. Between the subsequent polls, the red curve exhibits fluctuations, predominantly converging towards the solid black curve, reflecting incorporation of the available polling information into the current system state.

Notably, upon closer examination of Fig. 1, there are indications of periodic oscillations arising due to the periodic polling mechanism, even though the initial condition, $A_{-1} = A_0 = X(0)$, initially suppresses them. We will explore this effect in a more detail in a subsequent section.

3 Simulation methods

Model driven by the rates (2) could be simulated using one-step transition probability approach [49], with the condition that the time step is smaller than τ and the ratio between τ and the time step is an integer. The issue with this approach in the general case is that it is slow and it generates biased samples [50]. Gillespie method [50] could be employed as an approximation, but it would inaccurately represent one transition per every polling period, specifically the transition during which the crossover to the next polling period occurs. While the potential error is likely negligible, as misrepresentation becomes more noticeable only for small values of τ , but the delay effect induced by the polling mechanism is also smaller for smaller τ as well. Typically, for systems

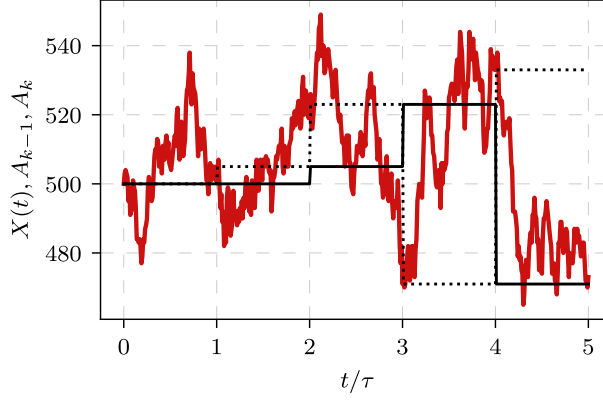


Figure 1: Dynamic interplay between the evolution of the system state $X(t)$ (red curve), the last announced poll outcome A_{k-1} representing the information about the system state available to agents (solid black curve), and the latest poll outcome A_k representing the information to be revealed in the future (black dotted curve). Simulation parameters were set as follows: $\varepsilon_0 = \varepsilon_1 = 2$, $\tau = 5 \cdot 10^{-3}$, $N = 10^3$, with initial conditions $A_{-1} = A_0 = X(0) = 500$.

with delays a modified next reaction method is used [50]. In our case, this method has performed approximately 4 times slower than the Gillespie method, but still, it has an advantage over the Gillespie method as it produces time series without misrepresenting any transition. In this section, we will discuss our adaptation of the Gillespie method for systems with delays, as well as introduce a macroscopic simulation method developed specifically for this model. We will also briefly touch upon capturing the model dynamics using a one-dimensional Markov chain.

3.1 Adapted Gillespie method for periodic polling with announcement delays

We propose the adapted Gillespie method by combining the best features of the Gillespie method and the next reaction method. Our adaption, outline given in Algorithm 1, is based on the Gillespie method, but introduces delay τ , the poll index k , and the k -th poll outcome A_k . In Step 5 of the algorithm, the delay mechanism is introduced by building on the idea of the internal reaction clock R from the next reaction method. This allows recalculation of the transition rates according to updated recent poll outcomes. The conditional statement in Step 5 of the algorithm checks if a poll should be conducted before the next transition (reaction, in the language of the original next reaction method). The while loop is used to handle an edge case when more than a single poll falls between 2 transitions. This edge arises often when $\tau \lesssim \frac{1}{N^2}$.

Python implementation of this method for the noisy voter model with delayed interactions is available at [51].

3.2 Macroscopic simulation method

This simulation method relies on an observation that the imitation term A_{k-1} remains constant throughout the polling interval. This enables us to introduce the effective individual agent transition rates that remain constant for the duration of the k -th polling period:

$$\varepsilon_1^{(k)} = \varepsilon_1 + A_{k-1}, \quad \varepsilon_0^{(k)} = \varepsilon_0 + (N - A_{k-1}). \quad (4)$$

These effective rates encompass both the truly independent transitions and the imitative behavior induced by the knowledge of the last announced poll outcome. This effect is somewhat reminiscent of the peer pressure exerted by zealots [42–46], although in our case the agents themselves still change their state, only their knowledge about the other agents remains conserved for the duration of the polling period. Consequently, the system-wide

Algorithm 1 Adapted Gillespie method

1. Set parameter values $\varepsilon_0, \varepsilon_1, N, \tau$. Set desired initial conditions $A_{-1}, X(0)$. Set the clock $t = 0$. Set the current polling period index $k = 0$. Conduct the initial poll, $A_0 = X(0)$.
 2. Calculate the system-wide transition rates λ^+ and λ^- according to Eq. (2).
 3. Calculate total transition rate $\lambda^T = \lambda^+ + \lambda^-$.
 4. Sample the time until the next reaction from an exponential distribution, $\Delta t \sim \text{Exp}(\lambda^T)$.
 5. While $t + \Delta t \geq (k + 1)\tau$:
 - Increment the polling period index $k \rightarrow k + 1$.
 - Conduct the k -th poll, $A_k = X(t)$.
 - Calculate the remaining time until the next reaction (according to the internal reaction clock) $R = \lambda^T [t + \Delta t - k\tau]$.
 - Update λ^+, λ^- according to Eq. (2). Update λ^T accordingly.
 - Adjust the time until the next reaction $\Delta t = \frac{R}{\lambda^T}$.
 - Update the clock $t \rightarrow k\tau$
 6. Update the clock $t \rightarrow t + \Delta t$.
 7. Sample uniformly distributed random value $r \sim \mathcal{U}(0, \lambda^T)$. If $r \leq \lambda^+$, set $X(t) = X(t - \Delta t) + 1$. Otherwise set $X(t) = X(t - \Delta t) - 1$.
 8. Go back to Step 4 or end the simulation.
-

transition rates during the polling period k would be given by

$$\lambda_k^+ = (N - X) \varepsilon_1^{(k)}, \quad \lambda_k^- = X \varepsilon_0^{(k)}. \quad (5)$$

The form of the system-wide transition rates suggests that each agent operates independently of others at all times, as they consider the available polling information. Upon the announcement of a new poll outcome, the transition rates get updated. Hence, we can approach the analysis of this model from the standpoint of an individual agent, and concentrating only on the current polling period.

In examining the behavior of a single agent, and given that the agent can occupy one of two possible states, the dynamics can be analyzed as a two-state Markov chain. Given the effective individual agent transition rates, Eq. (4), we can formulate the corresponding left stochastic transition matrix governing the transitions of an individual agent over an infinitesimally short time interval Δt :

$$\mathbf{Q} = \begin{pmatrix} 1 - \varepsilon_0^{(k)} \Delta t & \varepsilon_1^{(k)} \Delta t \\ \varepsilon_0^{(k)} \Delta t & 1 - \varepsilon_1^{(k)} \Delta t \end{pmatrix}. \quad (6)$$

By solving the eigenproblem with respect to \mathbf{Q} , we can infer that the probability to observe an agent in state “1” after m steps is given by

$$P_1(m|P_1(0)) = \frac{\varepsilon_1^{(k)}}{\varepsilon_0^{(k)} + \varepsilon_1^{(k)}} + \frac{\varepsilon_0^{(k)} P_1(0) - \varepsilon_1^{(k)} [1 - P_1(0)]}{\varepsilon_0^{(k)} + \varepsilon_1^{(k)}} \left[1 - (\varepsilon_0^{(k)} + \varepsilon_1^{(k)}) \Delta t \right]^m. \quad (7)$$

In the above $P_1(0)$ represents the “initial” condition of the Markov chain describing individual agent dynamics. Typically, $P_1(0)$ assumes a value of 1 if the agent under consideration is initially in the “1” state, or 0 otherwise. Additionally, it proves convenient to introduce notation $P_1(\infty)$ which denotes the stationary probability of

observing the agent in the “1” state,

$$P_1(\infty) = \frac{\varepsilon_1^{(k)}}{\varepsilon_0^{(k)} + \varepsilon_1^{(k)}} = \frac{\varepsilon_1 + A_{k-1}}{\varepsilon_0 + \varepsilon_1 + N}. \quad (8)$$

By taking the continuous time limit, i.e., letting $\Delta t \rightarrow 0$ and $m \rightarrow \infty$ (with $s = m\Delta t = \text{const}$), we obtain the conditional probability to observe an agent in the “1” state after time span s ,

$$P_1(s|P_1(0)) = P_1(\infty) + [P_1(0) - P_1(\infty)] \exp[-(\varepsilon_0 + \varepsilon_1 + N)s]. \quad (9)$$

We can use Eq. (9) to simulate the behavior of all N agents without resorting to the time-consuming direct simulation of the noisy voter model with periodic polling mechanism. Let $X(t)$ denote the system state at some arbitrary time t , and let s be a positive time increment such that $k\tau \leq t < t + s \leq (k+1)\tau$. Then, $X(t+s)$ can be sampled by adding two binomial random variables

$$X(t+s) = B_{1 \rightarrow 1}[X(t), P_1(s|1)] + B_{0 \rightarrow 1}[N - X(t), P_1(s|0)]. \quad (10)$$

In the expression above, $B_{1 \rightarrow 1}[\dots]$ corresponds to the count of agents that were in state “1” at time t and ended up in state “1” at time $t+s$. These agents may have remained in state “1” for the duration s , or they might have exited and subsequently returned to state “1”. In this setup, the specific evolution of an individual agent’s state doesn’t influence the outcome; only the initial and final states matter. Given there were $X(t)$ agents in state “1” at time t , and the probability that an agent starting in state “1” will end up in state “1” is given by $P_1(s|1)$, then $B_{1 \rightarrow 1}[\dots]$ is an outcome of $X(t)$ Bernoulli trials with a success probability of $P_1(s|1)$. Similarly, $B_{0 \rightarrow 1}[\dots]$ is an outcome of $N - X(t)$ Bernoulli trials with a success probability of $P_1(s|0)$.

This approach is most efficient when $t = k\tau$ and $s = \tau$, although finer-scale simulations are also possible for $s < \tau$. As long as the sampling period s encompasses a large number of transitions, this method proves to be more efficient than a direct simulation without compromising quality of the sampled time series. The detailed outline of the macroscopic simulation method is provided in Algorithm 2.

Algorithm 2 Macroscopic simulation method

1. Set parameter values $\varepsilon_0, \varepsilon_1, N, \tau$. Set desired initial conditions $A_{-1}, X(0)$. Set desired sampling period s (note that τ/s must be a positive integer). Set the clock $t = 0$. Set the current polling period index $k = 0$.
 2. Calculate the effective transition rates $\varepsilon_0^{(k)} = \varepsilon_0 + (N - A_{k-1}), \varepsilon_1^{(k)} = \varepsilon_1 + A_{k-1}$.
 3. Calculate the transition probabilities $P_1(s|1)$ and $P_1(s|0)$.
 4. Conduct the k -th poll, $A_k = X(t)$.
 5. Sample two binomial random values $B_{1 \rightarrow 1} \sim \text{Binom}[X(t), P_1(s|1)]$ and $B_{0 \rightarrow 1} \sim \text{Binom}[N - X(t), P_1(s|0)]$.
 6. Update the system state $X(t+s) = B_{1 \rightarrow 1} + B_{0 \rightarrow 1}$.
 7. Update the clock $t \rightarrow t + s$.
 8. If $t < (k+1)\tau$, go back to Step 5.
 9. Increment the polling period index $k \rightarrow k + 1$.
 10. Go back to Step 2 or end the simulation.
-

Python implementation of this method for the noisy voter model with delayed interactions is available at [51].

3.3 Comparison of the Monte-Carlo simulation methods

Both of the methods discussed earlier are Monte Carlo simulation methods. In order to obtain the temporal dependence of statistical moments or the stationary distribution, it is necessary to conduct multitude simulations using the same parameter set and subsequently average over the ensemble. Comparing the results obtained from simulations using these methods allows us to verify the validity of the macroscopic simulation method, which may not be immediately evident.

In the different simulations shown in Fig. 2 we keep N fixed and equal to 10^3 . We systematically vary the values of ε_i and τ parameters. While the initial conditions are purposefully selected to be very different in order to emphasize their importance on the values of mean and variance reached during the polling period. For all distinct cases the results of numerical simulations using both methods match reasonably well. So well that we are forced to make the red $\langle X(t) \rangle$ curve (obtained using the macroscopic simulation method) thicker. Fig. 2 (a) and (b) show how the mean and variance evolve for the base parameter set. The selected value of $\tau = 10^{-2}$ appears to be sufficient for the statistical moments to converge towards their stationary values; the mean approaches A_{-1} . As the delay τ is kept the same in Fig. 2 (c) and (d), the statistical moments still converge to their respective stationary values. In Fig. 2 (d) we can clearly observe localization phenomenon as the ensemble variance temporarily increases before converging to the stationary value. From Fig. 2 (e)-(h) it is evident that for shorter delay, $\tau = 10^{-3}$, the statistical moments fail to converge their respective stationary values: instead some intermediate values are reached. From Fig. 2 it is not clear what impact ε_i parameters have, while the initial conditions appear to be extremely important. This was expected as the macroscopic simulation method takes the effective rates as its input.

Producing Fig. 2 allows us to at least approximately compare the speed of the methods. It took couple of seconds to obtain all of the results using the macroscopic simulation method, while it took couple of minutes using the adapted Gillespie method. Given difference in the ensemble sizes, macroscopic simulation method produces the results roughly 10^2 times faster for the considered parameter sets and the selected time resolution. The difference in favor of the macroscopic simulation method was expected as it doesn't simulate individual transitions, only $X(t)$ values for desired t .

In the subsequent sections, we present the results obtained by simulating large a number of polling periods. Wherever feasible, we will use both simulation methods to reinforce validity of the obtained results as well as to show the equivalence of both Monte-Carlo simulation methods.

3.4 Semi-analytical approach based on the transition matrix for poll outcomes

If we focus only on the poll outcomes A_i , then the model under consideration reduces to the second-order Markov chain as the distribution of A_i depends on A_{i-1} and A_{i-2} . For finite N the phase space of the model is finite, for this reason we can reduce the second-order Markov chain to the first-order Markov chain. Let us derive an expression for the left stochastic transition matrix elements of this first-order Markov chain.

If we focus solely on the poll outcomes A_i , the model can be treated as a second-order Markov chain, as the distribution of A_i is conditioned on both A_{i-1} and A_{i-2} . In the case of a finite N , the phase space of the model is also finite. Consequently, we have the ability to further reduce the second-order Markov chain into a first-order Markov chain. Let us proceed to derive an expression for the left stochastic transition matrix elements of this first-order Markov chain.

Upon reducing the second-order Markov chain, we effectively introduce two-dimensional system state (A_i, A_{i-1}) . As $A_i \in [0, N]$, we can uniquely map the two-dimensional system state into one-dimensional index K_i :

$$K_i = 1 + A_i + (N + 1) \cdot A_{i-1}. \quad (11)$$

Index K_i corresponds to the row or column indices of the transition matrix \mathbf{T} . Given that $A_i \in [0, N]$, we have that $K_i \in [1, (N + 1)^2]$. This implies that the transition matrix will have $(N + 1)^4$ elements, although only

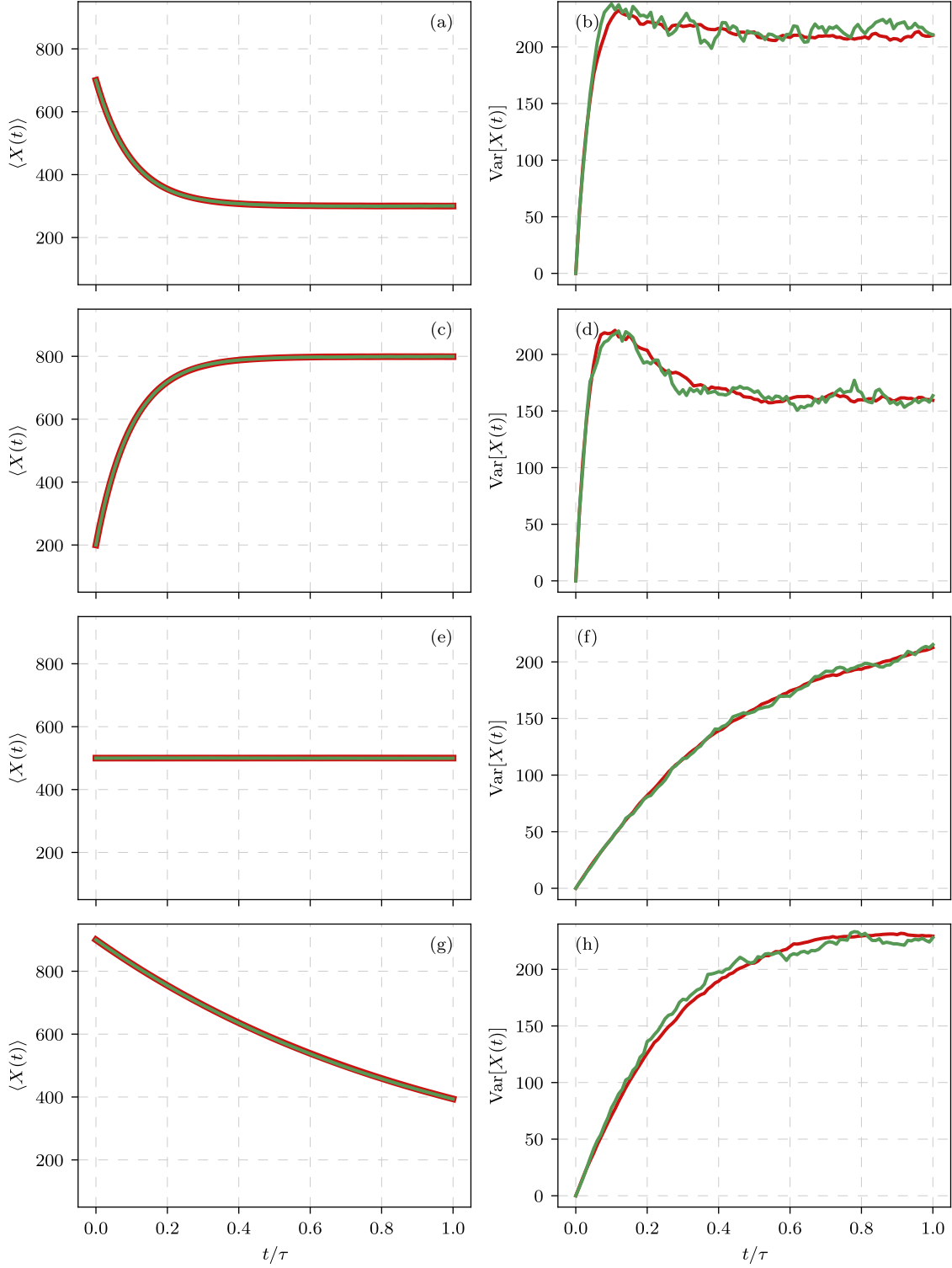


Figure 2: The evolution of statistical moments, mean ((a), (c), (e) and (g)) and variance ((b), (d), (f) and (h)), of numerically simulated ensembles. Different curves correspond to results obtained from the two simulation methods: red curve corresponds to the macroscopic simulation method (with ensemble size of 10^4), green curve corresponds to the adapted Gillespie method (with ensemble size of 10^3). Different pairs of plots were obtained with the different parameter sets: $\varepsilon_0 = \varepsilon_1 = 0.5$, $\tau = 10^{-2}$, $A_{-1} = 300$ and $A_0 = X(0) = 700$ ((a) and (b)); $\varepsilon_0 = \varepsilon_1 = 2$, $\tau = 10^{-2}$, $A_{-1} = 800$ and $A_0 = X(0) = 200$ ((c) and (d)); $\varepsilon_0 = 0.5$, $\varepsilon_1 = 0.5$, $\tau = 10^{-3}$ and $A_{-1} = A_0 = X(0) = 500$ ((e) and (f)); $\varepsilon_0 = \varepsilon_1 = 2$, $\tau = 10^{-3}$, $A_{-1} = 100$ and $A_0 = X(0) = 900$ ((g) and (h)). Shared parameter values: $N = 10^3$.

$(N+1)^2$ of them will be non-zero. The one-dimensional index K_i also uniquely maps to the two-dimensional system state (A_i, A_{i-1}) :

$$A_i = K_i - 1 - (N+1) \left\lfloor \frac{K_i - 1}{N+1} \right\rfloor, \quad A_{i-1} = \left\lfloor \frac{K_i - 1}{N+1} \right\rfloor. \quad (12)$$

In the indexing scheme introduced above, the (K, M) element of the left stochastic transition matrix \mathbf{T} representing $M \rightarrow K$ transition is given by

$$\begin{aligned} T_{K,M} &= P[M \rightarrow K] = \\ &= P \left[\left(M - 1 - (N+1) \left\lfloor \frac{M-1}{N+1} \right\rfloor, \left\lfloor \frac{M-1}{N+1} \right\rfloor \right) \rightarrow \left(K - 1 - (N+1) \left\lfloor \frac{K-1}{N+1} \right\rfloor, \left\lfloor \frac{K-1}{N+1} \right\rfloor \right) \right] = \\ &= \begin{cases} P \left[K - 1 - (N+1) \left\lfloor \frac{K-1}{N+1} \right\rfloor \mid \left\lfloor \frac{K-1}{N+1} \right\rfloor, \left\lfloor \frac{M-1}{N+1} \right\rfloor, \tau \right] & \text{if } \left\lfloor \frac{K-1}{N+1} \right\rfloor = M - 1 - (N+1) \left\lfloor \frac{M-1}{N+1} \right\rfloor, \\ 0 & \text{otherwise.} \end{cases} \end{aligned} \quad (13)$$

The conditional probability in the above is given by

$$P[A_{i+1}|A_i, A_{i-1}, \tau] = \sum_{k=0}^{A_{i+1}} p_{\text{Binom}}[k, A_i, P_1(\tau|1, A_{i-1})] \cdot p_{\text{Binom}}[A_{i+1} - k, N - A_i, P_1(\tau|0, A_{i-1})]. \quad (14)$$

In the above, $p_{\text{Binom}}(k, N, p)$ represents the probability mass function of the Binomial distribution with N trials and success probability p , while $P_1(\dots)$ corresponds to Eq. (9) additionally conditioned that the last announced poll outcome was A_{i-1} . The last announced poll outcome is not explicitly present in Eq. (9); however, it is implicitly present as a part of $P_1(\infty)$ and $\varepsilon_i^{(k)}$.

This approach provides an alternative semi-analytical method for simulating the model. The primary drawback of this method is that it is very time consuming, making it feasible only for small N . However, solving the eigenproblem with respect to \mathbf{T} allows obtaining the exact stationary distribution or the entire temporal evolution of the distribution for the selected parameters. The methods discussed earlier are faster, but they do not yield exact results.

Python implementation of this approach for the noisy voter model with delayed interactions is available at [51].

4 Stationary poll outcome distributions

As discussed in the previous section, the outcome of the next poll A_{k+1} for an arbitrary polling interval τ depends on the last announced poll outcome A_{k-1} and the system state at the start of the polling period $X(k\tau)$, which corresponds to A_k . Namely, the model behaves as a second-order Markov chain, yet it can be reduced to the first-order Markov chain for finite N . Determining eigenvectors and eigenvalues of the associated transition matrix yields the complete information about the evolution of the poll outcome distribution and also the exact stationary poll outcome distribution. However, an analytical solution of the eigenproblem is elusive, necessitating a numerical approach. The numerical solution of the eigenproblem is somewhat time-consuming and is only practical for small N . Alternatively, we can explore other approaches to derive analytical approximations for stationary poll outcome distributions. This objective drives the focus of this section.

From Eq. (10), it can be shown that the conditional mean of A_{k+1} with respect to A_k and A_{k-1} is given by

$$\langle A_{k+1} | A_k, A_{k-1} \rangle = \varphi_1 A_k + (1 - \varphi_1) \varphi_2 (\varepsilon_1 + A_{k-1}) \quad (15)$$

with $\varphi_1 = \exp[-(\varepsilon_0 + \varepsilon_1 + N)\tau]$ and $\varphi_2 = \frac{N}{\varepsilon_0 + \varepsilon_1 + N}$. Observe that if $\tau \rightarrow 0$, then $\varphi_1 \rightarrow 1$ and the conditional mean becomes independent of A_{k-1} . For small values of τ , the impact of the information delay should be minimal, as the poll outcomes are updated nearly as frequently as the system state. This suggests that the

delay would have a negligible effect on the poll outcomes. Consequently, when no or few transitions occur during a single polling period, which is often the case with $\tau \ll \frac{2}{N(\varepsilon_0 + \varepsilon_1 + N)}$, the model with delayed interactions should be almost equivalent to the noisy voter model. The equivalence implies that the stationary poll outcome distribution should be the same as the stationary distribution the noisy voter model would have, i.e., $A_\infty \sim \text{BetaBin}(N, \varepsilon_1, \varepsilon_0)$. This intuition is confirmed by numerical simulation (see Fig. 3).

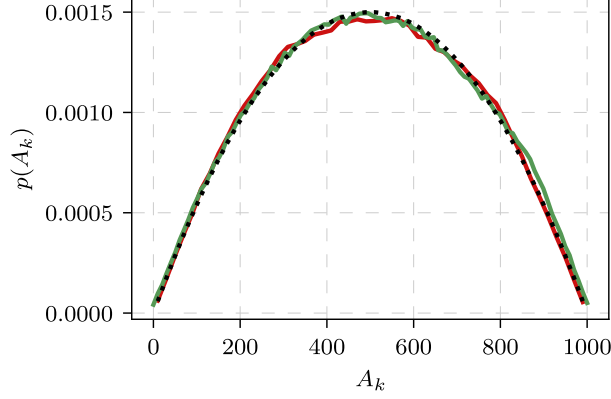


Figure 3: Stationary poll outcome distribution of the model with small τ . Numerical simulations were conducted using the macroscopic simulation method (red curve) and the adapted Gillespie method (green curve). Black dotted curve shows the probability mass function of the BetaBin($N, \varepsilon_1, \varepsilon_0$). Simulation parameters: $\varepsilon_0 = \varepsilon_1 = 2$, $\tau = 10^{-7}$, $N = 10^3$.

Likewise, in the large τ limit, i.e., $\tau \rightarrow \infty$, we have that $\varphi_1 \rightarrow 0$. Therefore, in this limit the conditional mean becomes independent of A_k . Intuitively, this suggests that in this limit, the model with delayed interactions behaves like two nearly independent Markov chains. One chain corresponds to the even poll indices, and the other to the odd poll indices. These Markov chains would be essentially identical in all aspects except for their initial conditions. It can be shown (see Appendix A) that the stationary mean in the large τ limit is given by

$$\langle A_\infty \rangle = \frac{N\varepsilon_1}{\varepsilon_0 + \varepsilon_1}. \quad (16)$$

For the large number of agents $N \gg (\varepsilon_0 + \varepsilon_1)$, the stationary variance in the large τ limit can be approximated by

$$\text{Var}[A_\infty] \approx \frac{N\varepsilon_1\varepsilon_0(2\varepsilon_0 + 2\varepsilon_1 + N)}{(\varepsilon_0 + \varepsilon_1)^2(2\varepsilon_0 + 2\varepsilon_1 + 1)}. \quad (17)$$

The expressions for the stationary moments suggest that the stationary poll outcome distribution in the large τ limit can be well approximated by BetaBin($N, 2\varepsilon_1, 2\varepsilon_0$) distribution. In Appendix A we have derived not only the exact stationary moments but have also determined their temporal evolution, i.e., we have obtained $\langle A_k \rangle$ and $\text{Var}[A_k]$ expressions with arbitrary k . In Fig. 4 we show that the obtained analytical expressions align with numerical simulation results rather well.

The results for the small τ and large τ limits prompt us to posit that the stationary distribution of the model with delayed interactions is a Beta-binomial for all possible τ . Only the shape parameters of the distribution change with τ according to some scaling law.

Let us average Eq. (15) over stationary distribution,

$$\langle A_\infty \rangle = \varphi_1 \langle A_\infty \rangle + (1 - \varphi_1) \varphi_2 (\varepsilon_1 + \langle A_\infty \rangle). \quad (18)$$

Solving the above with respect to $\langle A_\infty \rangle$, yields

$$\langle A_\infty \rangle = \frac{\varphi_2 \varepsilon_1}{1 - \varphi_2} = \frac{N\varepsilon_1}{\varepsilon_0 + \varepsilon_1}. \quad (19)$$

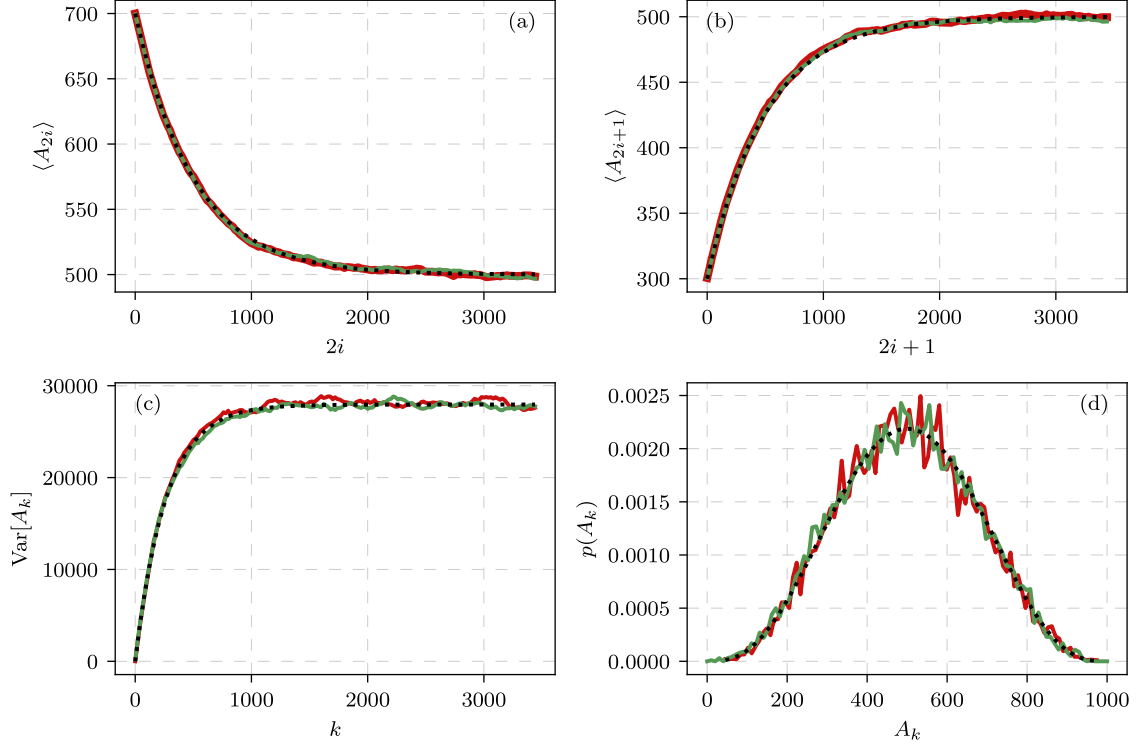


Figure 4: Evolution of the statistical moments and the stationary distribution of the model with large τ . (a) and (b) depict the evolution of the mean for even and odd poll indices, respectively, while (c) shows the evolution of the variance. (d) shows the stationary distribution. The red curve represents simulation results obtained using the macroscopic simulation method, while the green curve - results from the adapted Gillespie method. Black dotted curves correspond to analytical predictions: Eq. (44) for (a), Eq. (46) for (b), Eq. (51) for (c), and the probability mass function of $\text{BetaBin}(N, 2\varepsilon_1, 2\varepsilon_0)$ for (d). Simulation parameters: $\varepsilon_0 = \varepsilon_1 = 2$, $N = 10^3$, $\tau = 0.03$, $A_{-1} = 300$, and $A_0 = X(0) = 700$.

Which is identical to the stationary mean obtained for the small τ and large τ limits. The fact that $\langle A_\infty \rangle$ does not depend on τ indicates that both shape parameters of the stationary distribution follow the same scaling law $L(\tau)$. In other words, we have that

$$\hat{\alpha}(\tau) = \varepsilon_1 \cdot L(\tau) \quad \text{and} \quad \hat{\beta}(\tau) = \varepsilon_0 \cdot L(\tau), \quad (20)$$

here $\hat{\alpha}$ and $\hat{\beta}$ denote best estimates of the shape parameters of the Beta-binomial distribution. If $\hat{\alpha}$ and $\hat{\beta}$ would follow different scaling laws, $\langle A_\infty \rangle$ would depend on τ . In Fig. 5, we observe that $\hat{\alpha}/\varepsilon_1$ and $\hat{\beta}/\varepsilon_0$ obtained by numerical simulation align well, thus supporting the conclusions of the shared scaling law.

To facilitate further analysis, the goal of which is to determine $L(\tau)$, let us consider poll outcomes centered on the stationary mean,

$$\tilde{A}_k = A_k - \langle A_\infty \rangle. \quad (21)$$

Rewriting Eq. (15) with respect to \tilde{A}_k yields

$$\langle \tilde{A}_{k+1} | \tilde{A}_k, \tilde{A}_{k-1} \rangle = \varphi_1 \tilde{A}_k + (1 - \varphi_1) \varphi_2 \tilde{A}_{k-1}. \quad (22)$$

From Eq. (10), it follows that any deviations ξ_k of \tilde{A}_k from their conditional expected values $\langle \tilde{A}_k | \tilde{A}_{k-1}, \tilde{A}_{k-2} \rangle$ are conditionally independent and hence uncorrelated. We could assume that ξ_k follows a normal distribution with zero mean and stationary variance σ_ξ^2 . Under this assumption, Eq. (22) could be understood as a normal approximation to the macroscopic simulation method. Yet for further derivation this assumption is not strictly necessary. Let us then approximate \tilde{A}_k process by a stationary second order auto-regressive process [48] of the

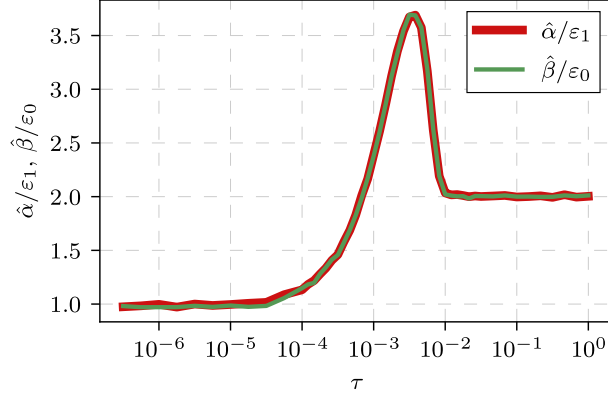


Figure 5: Scaling behavior of the normalized shape parameter estimates with respect to the polling period. Simulation parameters: $\varepsilon_0 = 2$, $\varepsilon_1 = 0.5$, $N = 10^3$.

the following form:

$$\tilde{A}_{k+1} = \varphi_1 \tilde{A}_k + (1 - \varphi_1) \varphi_2 \tilde{A}_{k-1} + \xi_{k+1}. \quad (23)$$

From Yule-Walker equations [48], we can determine stationary correlation between \tilde{A}_{k+1} and \tilde{A}_k denoted by ρ_1 and stationary correlation between \tilde{A}_{k+1} and \tilde{A}_{k-1} denoted by ρ_2 :

$$\rho_1 = \frac{\varphi_1}{1 - (1 - \varphi_1) \varphi_2}, \quad \rho_2 = (1 - \varphi_1) \varphi_2 + \frac{\varphi_1^2}{1 - (1 - \varphi_1) \varphi_2}. \quad (24)$$

And in turn, the stationary variance of the poll outcome distribution would be a solution of

$$\text{Var}[A_\infty] (1 - \varphi_1 \rho_1 - [1 - \varphi_1] \varphi_2 \rho_2) = \text{Var}[\xi_\infty]. \quad (25)$$

To proceed further let us determine $\text{Var}[\xi_\infty]$. From Eq. (10) with $s = \tau$, we have that

$$\begin{aligned} \text{Var}[\xi_k | A_k, A_{k-1}] &= \text{Var}[B_{1 \rightarrow 1} | A_k, A_{k-1}] + \text{Var}[B_{0 \rightarrow 1} | A_k, A_{k-1}] = \\ &= \psi_0 + \psi_1 \tilde{A}_k + \psi_2 \tilde{A}_{k-1} + \psi_{12} \tilde{A}_k \tilde{A}_{k-1} + \psi_{22} \tilde{A}_{k-1}^2. \end{aligned} \quad (26)$$

The coefficients above are given by

$$\begin{aligned} \psi_0 &= \frac{N \varepsilon_0 \varepsilon_1 (1 - \varphi_1^2)}{(\varepsilon_0 + \varepsilon_1)^2}, & \psi_1 &= \frac{(\varepsilon_0 - \varepsilon_1) \varphi_1 (1 - \varphi_1)}{\varepsilon_0 + \varepsilon_1}, & \psi_2 &= \frac{N (\varepsilon_0 - \varepsilon_1) (1 - \varphi_1)}{(\varepsilon_0 + \varepsilon_1 + N) (\varepsilon_0 + \varepsilon_1)}, \\ \psi_{12} &= -\frac{2 \varphi_1 (1 - \varphi_1)}{\varepsilon_0 + \varepsilon_1 + N}, & \psi_{22} &= -\frac{N (1 - \varphi_1)^2}{(\varepsilon_0 + \varepsilon_1 + N)^2}. \end{aligned} \quad (27)$$

Averaging Eq. (26) over the stationary distribution yields

$$\text{Var}[\xi_\infty] = \langle \text{Var}[\xi_k | A_k, A_{k-1}] \rangle = \psi_0 + (\psi_{12} \rho_1 + \psi_{22}) \text{Var}[A_\infty]. \quad (28)$$

Inserting Eq. (28) into Eq. (25) and solving it with respect to $\text{Var}[A_\infty]$ provides

$$\text{Var}[A_\infty] = \frac{\psi_0}{1 - (\varphi_1 + \psi_{12}) \rho_1 - (1 - \varphi_1) \varphi_2 \rho_2 - \psi_{22}}. \quad (29)$$

Taking $\tau \rightarrow 0$ and $\tau \rightarrow \infty$ limits of the above yields the expected results. For $\tau \rightarrow \infty$, Eq. 53 is recovered. Taking $\tau \rightarrow 0$ limit yields the expression for variance of the BetaBin($N, \varepsilon_1, \varepsilon_0$).

Solving

$$V(\tau) = \text{Var}[\text{BetaBin}\{N, \varepsilon_1 L(\tau), \varepsilon_0 L(\tau)\}], \quad (30)$$

where $V(\tau) = \text{Var}[A_\infty]$ is introduced just as a notational convenience chosen to emphasize the dependence of the stationary variance on τ , with respect to the scaling law yields

$$L(\tau) = \frac{\varepsilon_0 \varepsilon_1 N^2 - (\varepsilon_0 + \varepsilon_1)^2 V(\tau)}{(\varepsilon_0 + \varepsilon_1)^3 V(\tau) - \varepsilon_0 \varepsilon_1 (\varepsilon_0 + \varepsilon_1) N}. \quad (31)$$

As can be seen in Fig. 6, numerically simulated scaling behavior of $\hat{\alpha}/\varepsilon$ coincides rather well with the scaling law derived above.

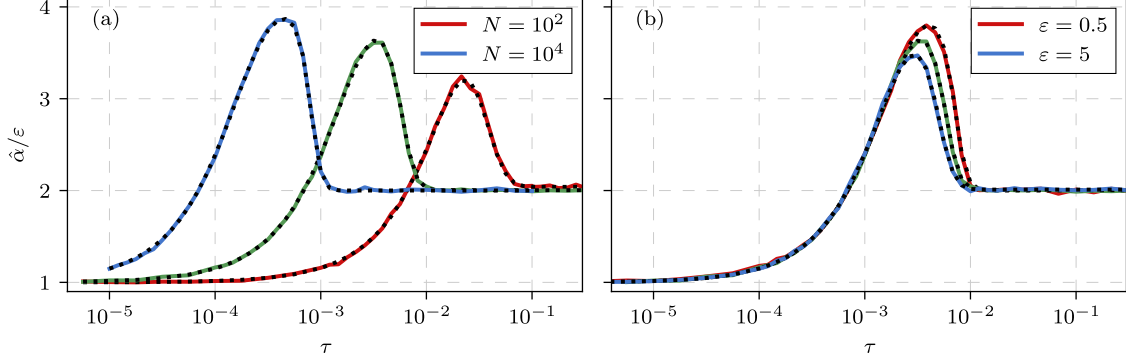


Figure 6: Scaling behavior of the normalized shape parameter estimate with respect to the polling period: when the number of agents vary (a) and when the independent transition rates vary (b). Solid colored curves correspond to the results obtained by numerical simulation. Black dotted curves indicate expected scaling behavior, given by Eq. (31). Base case simulation parameters (corresponds to the green curves in both (a) and (b)): $\varepsilon_0 = \varepsilon_1 = \varepsilon = 2$, $N = 10^3$. Legends indicate which parameter values differ from the base case if any.

As can be seen in Figs. 5 and 6, instead of observing a trivial sigmoid-like interpolation between the small τ limit and the large τ limit, we observe a non-trivial peak for some intermediate polling period τ_{\max} . The location of this peak can be estimated by solving maximization problem on the scaling law, Eq. (31), or by solving minimization problem on the stationary variance, Eq. (29). Either approach produces the same rather complicated form, but as usually we are interested in $N \gg (\varepsilon_0 + \varepsilon_1)$ case, then a reasonably compact approximation can be employed

$$\tau_{\max} \approx \frac{1}{2(\varepsilon_0 + \varepsilon_1 + N)} \ln \left(\frac{3N}{\varepsilon_0 + \varepsilon_1} \right). \quad (32)$$

In Fig. 7 we see that this approximation predicts the location of the peak of numerically simulated $\hat{\alpha}/\varepsilon_1$ rather well. Note that in the figure we have normalized the location of the peak to remove any dependency on ε_i , as only then the results of different numerical simulations would be expected to fall on a single curve. The normalization was done as follows: $\tilde{\tau}_{\max} = \frac{(\varepsilon_0 + \varepsilon_1 + N)}{N} \cdot \tau_{\max} + \frac{\ln(\varepsilon_0 + \varepsilon_1)}{2N}$.

From Eq. (31), we can also deduce the maximum value of the scaling law

$$L(\tau_{\max}) \approx 4 - \frac{6(1 + \varepsilon_0 + \varepsilon_1)}{1 + 3(\varepsilon_0 + \varepsilon_1) + \sqrt{3N}}. \quad (33)$$

As can be seen scaling law can have a maximum of at most 4. The maximum value is observed in the limits of $\varepsilon_i \rightarrow 0$ or $N \rightarrow \infty$. If instead $\varepsilon_i \gg \sqrt{N}$, the peak should notably diminish, but not disappear, as L_{\max} would be slightly above 2.

Let us also estimate the interval of polling periods for which the deviation from the sigmoid-like scaling behavior is observed. Interval bounds could be determined by formulating the problem with respect to the scaling law, but this would not yield any intuition on the nature of the peak. Therefore, let us approach this intuitively by exploring the behavior of expected value after a single polling period of an arbitrary length. From Eq. (10)

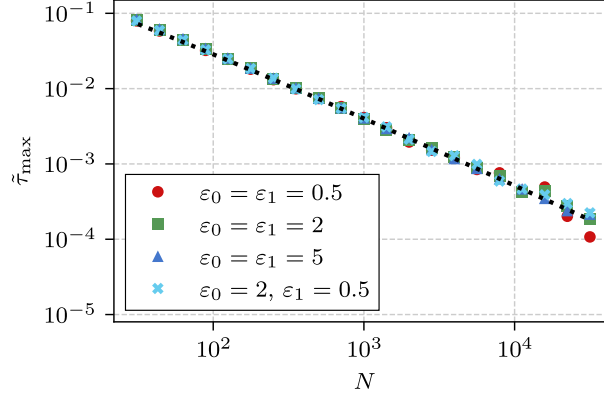


Figure 7: Normalized location of the peak in the numerically simulated $\hat{\alpha}(\tau)$ for different sets of ε_i and varying N . Outcomes of numerical simulations are depicted by varied symbols (corresponding ε_i values are given in the legend). The black dotted curve corresponds to an appropriately normalized Eq. (32).

with $k\tau = t$ and $s = \tau$, it is trivial to show that

$$\langle X(t + \tau) \rangle = \langle X(\infty) \rangle + \frac{\varepsilon_0^{(k)} X(t) - \varepsilon_1^{(k)} [N - X(t)]}{\varepsilon_0 + \varepsilon_1 + N} \exp[-(\varepsilon_0 + \varepsilon_1 + N)\tau]. \quad (34)$$

In the above $\langle X(\infty) \rangle$ stands for the stationary expected value, which is reached in the $\tau \rightarrow \infty$ limit. Let us find such τ_c for which $\langle X(t + \tau_c) \rangle$ reaches (i.e., is almost indistinguishable from) the stationary expected value:

$$\langle X(t + \tau_c) \rangle = \langle X(\infty) \rangle \pm \frac{1}{2}. \quad (35)$$

Solving the above for τ_c yields:

$$\tau_c = \frac{\ln(2|\langle X(\infty) \rangle - X(t)|)}{\varepsilon_0 + \varepsilon_1 + N}. \quad (36)$$

If we consider the largest possible distance between the initial and stationary states, $|\langle X(\infty) \rangle - X(t)| = N$, and the smallest $|\langle X(\infty) \rangle - X(t)| = 1$, we obtain:

$$\tau_c^{(1)} = \frac{\ln(2N)}{\varepsilon_0 + \varepsilon_1 + N}, \quad \text{and} \quad \tau_c^{(2)} = \frac{\ln(2)}{\varepsilon_0 + \varepsilon_1 + N}. \quad (37)$$

To verify whether these critical polling periods do indeed serve well as the interval bounds, let us put them into the scaling law, Eq. (31). We obtain:

$$L(\tau_c^{(1)}) \approx 2 + \frac{2}{1 + 2(\varepsilon_0 + \varepsilon_1)}, \quad \text{and} \quad L(\tau_c^{(2)}) \approx 2 + \frac{\varepsilon_0 + \varepsilon_1}{3N}. \quad (38)$$

It seems that $\tau_c^{(2)}$ is a really good estimate for lower interval bound, and the result improves as N grows larger. $\tau_c^{(1)}$ is a worse estimate, but may serve as a good rule of thumb for the determining the location of the upper bound. These derivations elucidate that the overshoot in $L(\tau)$, or alternatively the non-trivial decrease in $V(\tau)$, is caused by the tugging behavior between A_{k-1} and $X(k\tau)$ becoming observable not only in individual trajectories, but for all trajectories on average. But it remains unclear why the effect of the tugging behavior diminishes with large τ .

Expanding on a parallel line of reasoning, one may introduce additional τ_c by investigating instances when $\langle X(t + \tau_c) \rangle$ remains indistinguishable from $X(t)$. However, these additional τ_c do not provide any new information. τ_c corresponding to the smallest distance between initial condition and stationary value coincides with $\tau_c^{(2)}$, while τ_c corresponding to the largest distance coincides with we have discussed as a cutoff for the small τ limit.

5 Periodic fluctuations induced by the polling mechanism

Already in Fig. 1 we have observed hints of periodic fluctuations emerging from the model with delayed interactions. In Section 4 we have discussed that the model with delayed interactions effectively becomes a second-order Markov chain, which also suggests that the model could exhibit periodicity. Furthermore, delays themselves may also be the cause of periodic fluctuations.

As can be seen from a few sample trajectories shown in the plots on the left side of Fig. 8, the larger τ the more immediately evident the periodic fluctuations in $X(t)$ become. Power spectral densities of these time series (the plots on the right side of Fig. 8) indicate that the main fluctuation frequency is $f_k = \frac{1}{2}$ in the poll index space (hence, the subscript k), or $f = \frac{1}{2\tau}$ in the physical time space. Additional peaks are observed at harmonic frequencies of this main fluctuation frequency, therefore the only source of periodicity is the periodic polling mechanism itself.

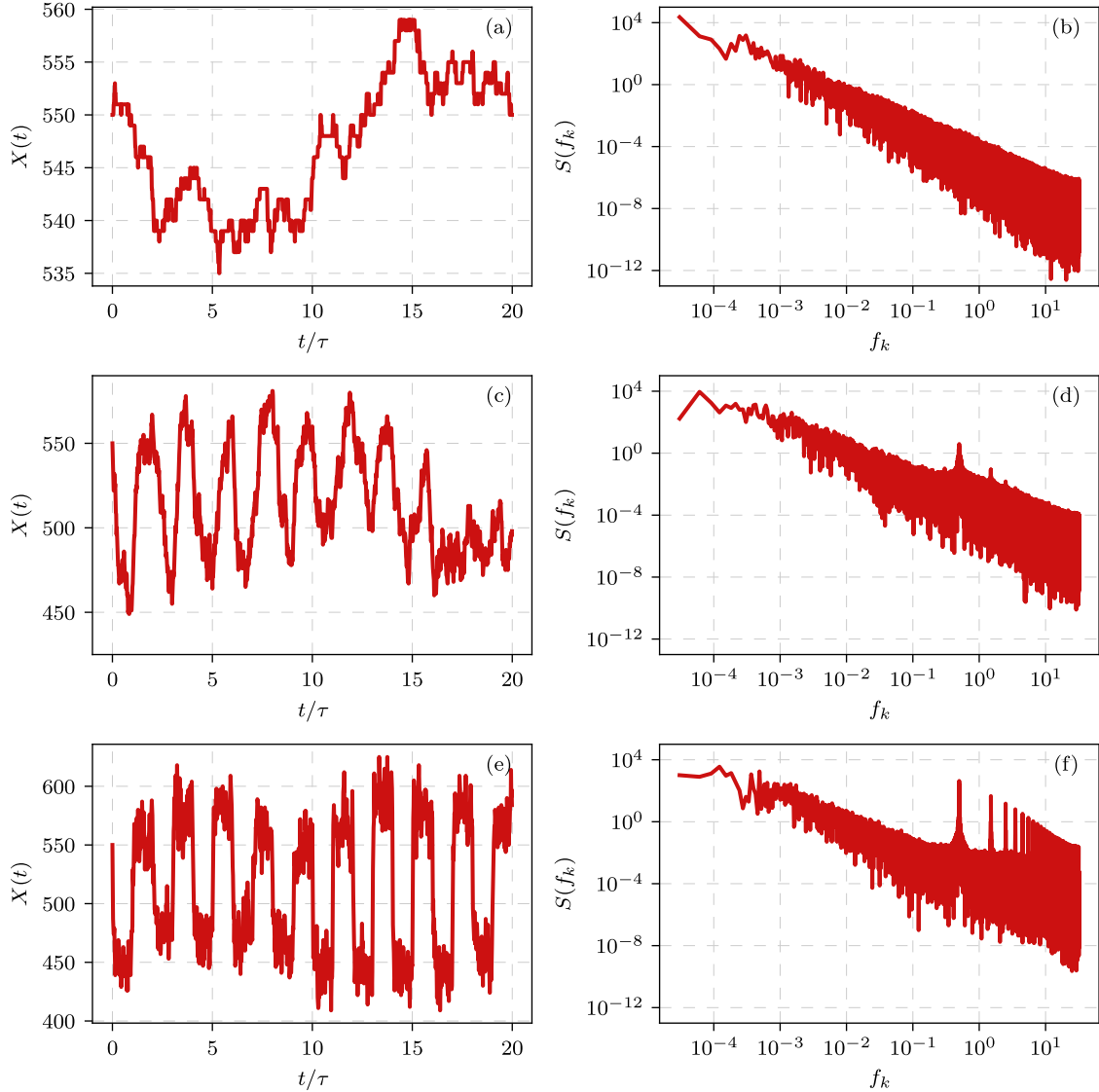


Figure 8: Fragment of time series obtained with different polling periods τ ((a), (c) and (e)), and the respective power spectral density in the poll index space ((b), (d) and (f)). Simulation parameters: $\varepsilon_0 = \varepsilon_1 = 2$, $N = 10^3$, $A_{-1} = 450$, $A_0 = X(0) = 550$ (in all cases), and $\tau = 3 \cdot 10^{-5}$ ((a) and (b)), $3 \cdot 10^{-3}$ ((c) and (d)), and $3 \cdot 10^{-2}$ ((e) and (f)).

The emergence of the periodic fluctuations therefore can be quantified by measuring the power spectral density

at $f_k = \frac{1}{2}$. Which is a squared absolute value of the Fourier transform at $f_k = \frac{1}{2}$:

$$S\left(f_k = \frac{1}{2}\right) = \frac{2}{M f_k^{(s)}} \left| \sum_{m=0}^{M-1} \tilde{X}\left(\frac{m}{f_k^{(s)}} \tau\right) \cdot \exp\left[-2i\pi \frac{f_k}{f_k^{(s)}} m\right] \right|^2. \quad (39)$$

In the above M is the length of the time series, $f_k^{(s)}$ is the sampling frequency in the poll index space (corresponds to the number of samples taken during a single polling period, e.g., $f_k^{(s)} = 100$ in Fig. 8), and $\tilde{X}(t) = \frac{X(t) - \langle X \rangle}{\sqrt{\text{Var}[X]}}$, i.e., standardized $X(t)$.

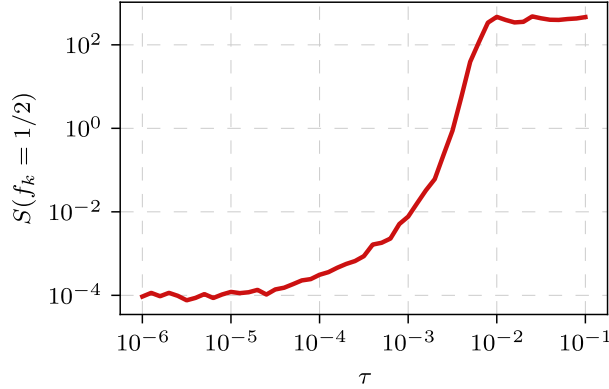


Figure 9: Power spectral density at the frequency corresponding to the observed periodic fluctuations, $S(f_k = \frac{1}{2})$, of numerically simulated time series with different polling periods τ . Simulation parameters: $\varepsilon_0 = \varepsilon_1 = 2$, $N = 10^3$.

The scaling of $S(f_k = \frac{1}{2})$ concerning τ has a trivial sigmoid shape (see Fig. 9). For small τ , i.e., $\tau \lesssim \frac{2}{N(\varepsilon_0 + \varepsilon_1 + N)}$, the system does not manage to incorporate the information potentially revealed by polls. Therefore, no opinion swings are observed. Small increases in τ do little to help the system incorporate the polling information. Therefore, in this range, we observe a slow growth of $S(f_k = \frac{1}{2})$. For sufficiently large τ , i.e., $\tau \gg \tau_c^{(1)}$, further increases in τ have no effect observable effect, because the system already has had enough time to incorporate all of the available polling information. For intermediate τ , even a small increase in τ allows for more polling information to be incorporated, but the incorporation is never complete. Consequently, in this range $S(f_k = \frac{1}{2})$ grows rapidly, likely exponentially due to the exponential dependence on τ in Eq. (9). No special scaling behavior is observed close to $\tau_c^{(2)}$, where the peak in the scaling law starts.

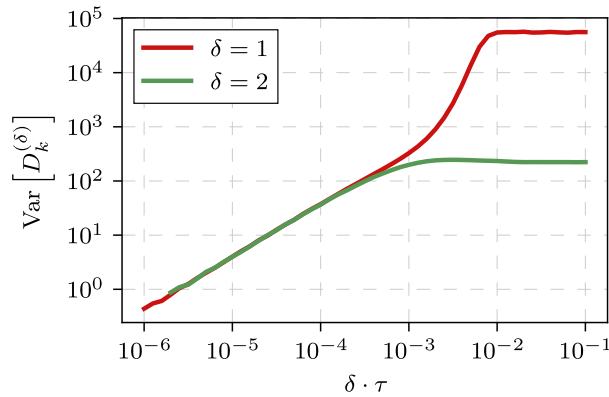


Figure 10: Variance of the differences between the consecutive poll outcomes, $D_k^{(1)}$, and the differences between the next-consecutive poll outcomes, $D_k^{(2)}$, with different polling periods τ . Simulation parameters: $\varepsilon_0 = \varepsilon_1 = 2$, $N = 10^3$.

Alternatively, the periodic fluctuations could be quantified by looking at the distribution of differences (or

swings) between the consecutive polls:

$$D_k^{(\delta)} = A_k - A_{k-\delta}. \quad (40)$$

For the periodic fluctuations to become apparent the swings between the consecutive poll outcomes, $D_k^{(1)}$, need to become relatively large in comparison to the swings between the next-consecutive poll outcomes, $D_k^{(2)}$. As can be seen in Fig. 10, the variance of both $D_k^{(1)}$ and $D_k^{(2)}$ initially grows with τ , but $D_k^{(2)}$ saturates sooner, at approximately $\tau_c^{(2)}$. Saturation of $D_k^{(1)}$ occurs for larger τ , which roughly corresponds to $\tau_c^{(1)}$. So difference in the scaling behavior of the swing variances seems to be related to the peak observed in $L(\tau)$.

6 Conclusions

We have examined the implications of information delays arising from the periodic polling mechanism on the opinion formation process. We have achieved this by integrating the periodic polling mechanism into the noisy voter model. Specifically, we have replaced instantaneous imitative interactions with imitative interactions mediated through periodic polls. Consistent with real-world scenarios, we have assumed a delay in announcing poll outcomes. Additionally, we have also aligned the announcement delay with the polling period. The proposed generalization constitutes a novel type of latency contrasting the one proposed in [37]. Namely, in [37] it was assumed that the agents freeze their opinion for some fixed duration, while in the proposed generalization the perception of society as a whole is being frozen for duration of the polling period instead.

The generalized model reveals non-trivial phenomenology. Namely, in the short polling period limit, the generalized model is almost equivalent to the noisy voter model. In the long polling period limit, the generalized model retains approximately the Beta-binomial form of the stationary distribution, but it becomes narrower (stationary variance is halved) in comparison to what would be expected from the noisy voter model. Yet the transition between the two limits exhibits non-monotonicity. Namely, the stationary variance reaches its minimum, or the distribution shape parameters reach their maximum, for some intermediate polling period. These results were obtained both numerically and analytically.

For the purposes of numerical simulation, we have adapted the Gillespie method, which is typically used for processes without delays [50], to incorporate delays specific to the generalized model. For short polling periods, this method has served us well, but as the polling periods become longer, the simulation using this method becomes increasingly more time-consuming, because every transition needs to be explicitly simulated. To address this issue, we have developed a macroscopic simulation method, which allows us to simulate just the poll outcomes. Furthermore, the proposed macroscopic simulation method has enabled partial analytical treatment of the model. Python implementation of all the algorithms used to simulate the generalized model (including the semi-analytical approach) is available at [51].

Given that delays themselves may contribute to periodic fluctuations, we have investigated the emergence of periodicity within the generalized model. We have found that the power spectral density peaks at the frequency corresponding to the doubled polling period and at other harmonic frequencies. The magnitude of the peak at the first harmonic frequency scales predictably, following a monotonic sigmoid-like function of the polling period. We have also examined the scaling of the variance of the poll outcome swings. We have found that for short polling periods, the variance of the consecutive and the next-consecutive poll swings grows together, but the variance of the next-consecutive poll swings saturates earlier and does so at the lower value. The polling period at which the separation is observed roughly coincides with the start of non-trivial behavior in the distribution shape parameter scaling law. Saturation of the variance of the consecutive poll swings roughly coincides with the long polling period limit.

The proposed generalization of the noisy voter model holds promise for further refinement and a more comprehensive investigation of the demonstrated rich phenomenology. Also, while we were able to predict the location of the peak in the scaling law behind the distribution shape parameters, we were not able to provide detailed explanation for the non-monotonic behavior. This could be addressed by further probing of the generalized

model. The proposed generalization could also serve as a foundational framework for analytically probing other types of societal latency in noisy voter models. As mentioned, we explore a novel kind of latency, which could be also introduced into other models of opinion dynamics, or other generalizations of the voter model. Additionally, this extension may prove instrumental in the development of domain-specific ARCH-like models for opinion dynamics, branching away from the traditional applications in economics and finance [52–54].

Author contributions

AK: Conceptualization, Methodology, Software, Validation, Writing, Visualization. **RA:** Methodology, Software, Validation, Writing. **MR:** Conceptualization, Methodology, Validation, Writing, Supervision. **FI:** Conceptualization, Writing, Supervision, Project administration.

References

- [1] T. Muller, M. Lauk, M. Reinhard, A. Hetzel, C. H. Lücking, J. Timmer, Estimation of delay times in biological systems, *Annals of Biomedical Engineering* 31 (2003) 1423–1439. doi:10.1114/1.1617984.
- [2] M. Dehghan, R. Salehi, Solution of a nonlinear time-delay model in biology via semi-analytical approaches, *Computer Physics Communications* 181 (2010) 1255–1265. doi:10.1016/j.cpc.2010.03.014.
- [3] A. Sargood, E. A. Gaffney, A. L. Krause, Fixed and distributed gene expression time delays in reaction-diffusion systems, *Bulletin of Mathematical Biology* 84 (2022). doi:10.1007/s11538-022-01052-0.
- [4] D. Moreno, J. Wooders, Prices, delay, and the dynamics of trade, *Journal of Economic Theory* 104 (2002) 304–339. doi:10.1006/jeth.2001.2822.
- [5] C. Ahlin, P. Bose, Bribery, inefficiency, and bureaucratic delay, *Journal of Development Economics* 84 (2007) 465–486. doi:10.1016/j.jdeveco.2005.12.002.
- [6] A. Kononovicius, J. Ruseckas, Order book model with herding behavior exhibiting long-range memory, *Physica A* 525 (2019) 171–191. doi:10.1016/j.physa.2019.03.059.
- [7] C. Aghamolla, T. Hashimoto, Information arrival, delay, and clustering in financial markets with dynamic freeriding, *Journal of Financial Economics* 138 (2020) 27–52. doi:10.1016/j.jfineco.2020.04.011.
- [8] J. Foss, A. Longtin, B. Mensour, J. Milton, Multistability and delayed recurrent loops, *Physical Review Letters* 76 (1996) 708–711. doi:10.1103/physrevlett.76.708.
- [9] M. K. S. Yeung, S. H. Strogatz, Time delay in the Kuramoto model of coupled oscillators, *Physical Review Letters* 82 (1999) 648–651. doi:10.1103/physrevlett.82.648.
- [10] K. Pyragas, Delayed feedback control of chaos, *Philosophical Transactions of the Royal Society A: Mathematical, Physical and Engineering Sciences* 364 (2006) 2309–2334. doi:10.1098/rsta.2006.1827.
- [11] N. C. Pati, Bifurcations and multistability in a physically extended Lorenz system for rotating convection, *The European Physical Journal B* 96 (2023). doi:10.1140/epjb/s10051-023-00585-0.
- [12] M. E. Inchiosa, A. R. Bulsara, L. Gammaitoni, Higher-order resonant behavior in asymmetric nonlinear stochastic systems, *Physical Review E* 55 (1997) 4049–4056. doi:10.1103/PhysRevE.55.4049.
- [13] T. Ohira, T. Yamane, Delayed stochastic systems, *Physical Review E* 61 (2000) 1247–1257. doi:10.1103/PhysRevE.61.1247.
- [14] C. Rouvas-Nicolis, G. Nicolis, Stochastic resonance, *Scholarpedia* 2 (2007) 1474. doi:10.4249/scholarpedia.1474.
- [15] P. Ashcroft, T. Galla, Pattern formation in individual-based systems with time-varying parameters, *Physical Review E* 88 (2013) 062104. doi:10.1103/PhysRevE.88.062104.
- [16] J. D. Touboul, The hipster effect: When anti-conformists all look the same, *Discrete & Continuous Dynamical Systems B* 24 (2019) 4379–4415. doi:10.3934/dcdsb.2019124.
- [17] R. Dieci, S. Mignot, F. Westerhoff, Production delays, technology choice and cyclical cobweb dynamics, *Chaos, Solitons & Fractals* 156 (2022) 111796. doi:10.1016/j.chaos.2022.111796.
- [18] S. Roy, S. Nag Chowdhury, S. Kundu, G. K. Sar, J. Banerjee, B. Rakshit, P. C. Mali, M. Perc, D. Ghosh, Time delays shape the eco-evolutionary dynamics of cooperation, *Scientific Reports* 13 (2023). doi:10.1038/s41598-023-41519-1.
- [19] S. Galam, Sociophysics: A review of Galam models, *International Journal of Modern Physics C* 19 (2008) 409. doi:10.1142/S0129183108012297.
- [20] C. Castellano, S. Fortunato, V. Loreto, Statistical physics of social dynamics, *Reviews of Modern Physics* 81 (2009) 591–646. doi:10.1103/RevModPhys.81.591.

- [21] F. Abergel, H. Aoyama, B. Chakrabarti, A. Chakraborti, N. Deo, D. Raina, I. Vodenska (Eds.), *Econophysics and sociophysics: Recent progress and future directions*, Springer International Publishing, 2017. doi:10.1007/978-3-319-47705-3.
- [22] A. Jedrzejewski, K. Sznajd-Weron, Statistical physics of opinion formation: Is it a SPOOF?, *Comptes Rendus Physique* 20 (2019) 244–261. doi:10.1016/j.crhy.2019.05.002.
- [23] S. Redner, Reality inspired voter models: a mini-review, *Comptes Rendus Physique* 20 (2019) 275–292. doi:10.1016/j.crhy.2019.05.004.
- [24] H. Noorazar, Recent advances in opinion propagation dynamics, *The European Physical Journal Plus* 135 (2020) 521. doi:10.1140/epjp/s13360-020-00541-2.
- [25] A. F. Peralta, J. Kertesz, G. Iniguez, Opinion dynamics in social networks: From models to data, available as arXiv:2201.01322 [physics.soc-ph] (2022). doi:10.48550/arXiv.2201.01322.
- [26] P. Clifford, A. Sudbury, A model for spatial conflict, *Biometrika* 60 (1973) 581–588. doi:10.1093/biomet/60.3.581.
- [27] T. Liggett, *Stochastic interacting systems: Contact, voter, and exclusion processes*, Springer, 1999.
- [28] M. Starnini, A. Baronchelli, R. Pastor-Satorras, Ordering dynamics of the multi-state voter model, *Journal of Statistical Mechanics: Theory and Experiment* 2012 (2012) P10027. doi:10.1088/1742-5468/2012/10/p10027.
- [29] A. Kononovicius, V. Gontis, Three state herding model of the financial markets, *EPL* 101 (2013) 28001. doi:10.1209/0295-5075/101/28001.
- [30] F. Vazquez, E. S. Loscar, G. Baglietto, A multi-state voter model with imperfect copying, *Physical Review E* 100 (2019) 042301. doi:10.1103/PhysRevE.100.042301.
- [31] L. B. Granovsky, N. Madras, The noisy voter model, *Stochastic Processes and their Applications* 55 (1995) 23–43. doi:10.1016/0304-4149(94)00035-R.
- [32] A. P. Kirman, Ants, rationality and recruitment, *Quarterly Journal of Economics* 108 (1993) 137–156. doi:10.2307/2118498.
- [33] J. Fernandez-Gracia, K. Suchecki, J. J. Ramasco, M. San Miguel, V. M. Eguiluz, Is the voter model a model for voters?, *Physical Review Letters* 112 (2014) 158701. doi:10.1103/PhysRevLett.112.158701.
- [34] F. Sano, M. Hisakado, S. Mori, Mean field voter model of election to the house of representatives in Japan, in: *JPS Conference Proceedings*, Vol. 16, The Physical Society of Japan, 2017, p. 011016. doi:10.7566/JPSCP.16.011016.
- [35] D. Braha, M. A. M. de Aguiar, Voting contagion: Modeling and analysis of a century of U.S. presidential elections, *PLOS ONE* 12 (2017) e0177970. doi:10.1371/journal.pone.0177970.
- [36] A. Kononovicius, Empirical analysis and agent-based modeling of Lithuanian parliamentary elections, *Complexity* 2017 (2017) 7354642. doi:10.1155/2017/7354642.
- [37] R. Lambiotte, J. Saramaki, V. D. Blondel, Dynamics of latent voters, *Physical Review E* 79 (2009) 046107. doi:10.1103/PhysRevE.79.046107.
- [38] O. Artime, A. F. Peralta, R. Toral, J. Ramasco, M. San Miguel, Aging-induced continuous phase transition, *Physical Review E* 98 (2018) 032104. doi:10.1103/PhysRevE.98.032104.
- [39] A. F. Peralta, N. Khalil, R. Toral, Ordering dynamics in the voter model with aging, *Physica A* 552 (2020) 122475. doi:10.1016/j.physa.2019.122475.
- [40] H. Chen, S. Wang, C. Shen, H. Zhang, G. Bianconi, Non-markovian majority-vote model, *Physical Review E* 102 (2020) 062311. doi:10.1103/PhysRevE.102.062311.
- [41] L. C. F. Latoski, W. G. Dantas, J. J. Arenzon, Curvature-driven growth and interfacial noise in the voter model with self-induced zealots, *Physical Review E* 106 (2022) 014121, available as arXiv:2204.03402 [cond-mat.stat-mech]. doi:10.1103/PhysRevE.106.014121.
- [42] S. Galam, F. Jacobs, The role of inflexible minorities in the breaking of democratic opinion dynamics, *Physica A* 381 (2007) 366–376. doi:10.1016/j.physa.2007.03.034.
- [43] M. Mobilia, A. Petersen, S. Redner, On the role of zealotry in the voter model, *Journal of Statistical Mechanics* 2007 (2007) P08029. doi:10.1088/1742-5468/2007/08/p08029.
- [44] A. Kononovicius, V. Gontis, Control of the socio-economic systems using herding interactions, *Physica A* 405 (2014) 80–84. doi:10.1016/j.physa.2014.03.003.
- [45] N. Khalil, M. San Miguel, R. Toral, Zealots in the mean-field noisy voter model, *Physical Review E* 97 (2018) 012310. doi:10.1103/PhysRevE.97.012310.
- [46] P. G. Meyer, R. Metzler, Time scales in the dynamics of political opinions and the voter model, *New Journal of Physics* 26 (2024) 023040. doi:10.1088/1367-2630/ad27bc.
- [47] M. Levene, T. Fenner, A stochastic differential equation approach to the analysis of the 2017 and 2019 UK general election polls, *International Journal of Forecasting* (2021). doi:10.1016/j.ijforecast.2021.02.002.
- [48] P. J. Brockwell, R. A. Davis, Springer, 1991. doi:10.1007/978-1-4419-0320-4.
- [49] N. G. van Kampen, *Stochastic process in physics and chemistry*, North Holland, Amsterdam, 2007.

- [50] D. F. Anderson, A modified next reaction method for simulating chemical systems with time dependent propensities and delays, *The Journal of Chemical Physics* 127 (2007) 214107. doi:10.1063/1.2799998.
- [51] <https://github.com/akononovicius/poll-delayed-noisy-voter-model>
- [52] L. Giraitis, R. Leipus, D. Surgailis, ARCH(∞) models and long memory, in: T. G. Anderson, R. A. Davis, J. Kreis, T. Mikosh (Eds.), *Handbook of Financial Time Series*, Springer Verlag, Berlin, 2009, pp. 71–84. doi:10.1007/978-3-540-71297-8_3.
- [53] N. Chalissery, S. Anagreh, M. Nishad T., M. I. Tabash, Mapping the trend, application and forecasting performance of asymmetric garch models: A review based on bibliometric analysis, *Journal of Risk and Financial Management* 15 (2022) 406. doi:10.3390/jrfm15090406.
- [54] T. Bollerslev, The story of GARCH: A personal odyssey, *Journal of Econometrics* 234 (2023) 96–100. doi:10.1016/j.jeconom.2023.01.015.

A The large τ limit

Starting from the premise of the macroscopic simulation method introduced in Section 3.2, we can explore the statistical characteristics of the model in the limit of large τ . Polling period τ should be as large as it would make the outcome A_{k+1} effectively independent of A_k . This can be achieved when $\tau \gg \frac{1}{\varepsilon_0 + \varepsilon_1 + N}$. For $\tau \gg \frac{1}{\varepsilon_0 + \varepsilon_1 + N}$, we have that $P_1(\tau|0) \approx P_1(\infty)$ and $P_1(\tau|1) \approx P_1(\infty)$. As in this limit the next poll outcome A_{k+1} depends only on A_{k-1} , we can now analyze the model with delayed interactions not as a second-order Markov chain, but instead as two independent first-order Markov chains. Because these two chains are identical in all regards except the initial conditions, let us limit the detailed derivations to the chain for even poll indices.

Let $p_\tau(x|u)$ denote the probability of observing $A_{k+1} = x$ given that $A_{k-1} = u$, i.e., the transition probability between the outcomes of subsequent even or odd polls. The distribution of the k -th poll outcome can be obtained through a recursive relationship

$$p_{k+1}(x) = \sum_{u=0}^N p_\tau(x|u) p_{k-1}(u), \quad (41)$$

with the initial conditions

$$p_0(x) = \delta(x - A_0), \quad p_{-1}(x) = \delta(x - A_{-1}). \quad (42)$$

In the expression above, $\delta(x)$ denotes a Kronecker delta function, its value is 1 if $x = 0$ and is 0 otherwise. Then both $P_1(\tau|0)$ and $P_1(\tau|1)$ are close to $P_1(\infty)$, $p_\tau(x|u)$ corresponds to a Binomial distribution probability mass function with N trials and the success probability $P_1(\infty)$, which is implicitly a function of $u = A_{k-1}$, Eq. (8). Obtaining a general analytical expressions for $p_i(x)$ or $p_\infty(x)$ doesn't seem feasible, but this problem could be approached from a numerical perspective. Approach discussed in Section 3.4 would yield similar results to iterating Eq. (41), but the approach discussed in Section 3.4 would not be limited to the large τ values. Instead let us focus on deriving expressions for the evolution of mean and variance of the poll outcome distribution.

As the poll outcome distributions are linked via recursive relationship, Eq. (41), we can show that the mean will satisfy another recursive relationship

$$\langle A_{k+1} \rangle = \sum_{x=0}^N x p_{k+1}(x) = \sum_{u=0}^N \left[\left(\sum_{x=0}^N x p_\tau(x|u) \right) p_{k-1}(u) \right] = \sum_{u=0}^N \frac{N(\varepsilon_1 + u)}{\varepsilon_0 + \varepsilon_1 + N} p_{k-1}(u) = \frac{N(\varepsilon_1 + \langle A_{k-1} \rangle)}{\varepsilon_0 + \varepsilon_1 + N}. \quad (43)$$

For even poll indices, this recursive form can be rewritten as

$$\langle A_k \rangle = \langle A_\infty \rangle + (A_0 - \langle A_\infty \rangle) \left(\frac{N}{\varepsilon_0 + \varepsilon_1 + N} \right)^{k/2}, \quad (44)$$

where k is the poll index, and $\langle A_\infty \rangle$ is the stationary mean,

$$\langle A_\infty \rangle = \frac{N\varepsilon_1}{\varepsilon_0 + \varepsilon_1}. \quad (45)$$

Repeating the same derivation for the odd poll indices, we obtain

$$\langle A_k \rangle = \langle A_\infty \rangle + (A_{-1} - \langle A_\infty \rangle) \left(\frac{N}{\varepsilon_0 + \varepsilon_1 + N} \right)^{(k+1)/2}. \quad (46)$$

In Fig. 4 (a) and (b) we see that the analytical expressions for the mean of even and odd k polls match the numerical simulations rather well.

The recursive relationship for the second raw moment is somewhat more complicated

$$\begin{aligned}\langle A_{k+1}^2 \rangle &= \sum_{x=0}^N x^2 p_{k+1}(x) = \sum_{u=0}^N \left[\left(\sum_{x=0}^N x^2 p_T(x|u) \right) p_{k-1}(u) \right] = \\ &= \frac{N [\varepsilon_1 (\varepsilon_0 + N + \varepsilon_1 N) + (\varepsilon_0 - \varepsilon_1 + N + 2\varepsilon_1 N) \langle A_{k-1} \rangle + (N-1) \langle A_{k-1}^2 \rangle]}{(\varepsilon_0 + \varepsilon_1 + N)^2}.\end{aligned}\quad (47)$$

For even poll indices, this recursive form can be rewritten as

$$\langle A_k^2 \rangle = A_\infty^{(2)} + [A_0^2 - A_\infty^{(2)} - A_{\text{mid}}^{(2)}] \left[\frac{N(N-1)}{(\varepsilon_0 + \varepsilon_1 + N)^2} \right]^{k/2} + A_{\text{mid}}^{(2)} \left[\frac{N}{\varepsilon_0 + \varepsilon_1 + N} \right]^{k/2}, \quad (48)$$

with

$$A_{\text{mid}}^{(2)} = (A_0 - \langle A_\infty \rangle) \frac{\varepsilon_0 - \varepsilon_1 + N + 2\varepsilon_1 N}{\varepsilon_0 + \varepsilon_1 + 1}, \quad (49)$$

$$A_\infty^{(2)} = \langle A_\infty^2 \rangle = \frac{N\varepsilon_1 [(\varepsilon_0 + N + \varepsilon_1 N)(\varepsilon_0 + \varepsilon_1) + (\varepsilon_0 - \varepsilon_1 + N + 2\varepsilon_1 N)N]}{(\varepsilon_0 + \varepsilon_1) [(\varepsilon_0 + \varepsilon_1 + N)^2 - N(N-1)]}. \quad (50)$$

Given the expression for the second raw moment, the variance for the even poll indices k can be shown to be

$$\begin{aligned}\text{Var}[A_k] &= \langle A_k^2 \rangle - \langle A_k \rangle^2 = \text{Var}[A_\infty] + \left(A_0^2 - A_\infty^{(2)} - A_{\text{mid}}^{(2)} \right) \left[\frac{N(N-1)}{(\varepsilon_0 + \varepsilon_1 + N)^2} \right]^{k/2} + \\ &+ \left[A_{\text{mid}}^{(2)} - 2\langle A_\infty \rangle (A_0 - \langle A_\infty \rangle) \right] \left(\frac{N}{\varepsilon_0 + \varepsilon_1 + N} \right)^{k/2} - (A_0 - \langle A_\infty \rangle)^2 \left(\frac{N}{\varepsilon_0 + \varepsilon_1 + N} \right)^{2k}.\end{aligned}\quad (51)$$

Repeating the same derivation for the odd poll indices k , we see that

$$\begin{aligned}\text{Var}[A_k] &= \text{Var}[A_\infty] + \left(A_{-1}^2 - A_\infty^{(2)} - A_{\text{mid}}^{(2)} \right) \left[\frac{N(N-1)}{(\varepsilon_0 + \varepsilon_1 + N)^2} \right]^{(k+1)/2} + \\ &+ \left[A_{\text{mid}}^{(2)} - 2\langle A_\infty \rangle (A_{-1} - \langle A_\infty \rangle) \right] \left(\frac{N}{\varepsilon_0 + \varepsilon_1 + N} \right)^{(k+1)/2} - (A_{-1} - \langle A_\infty \rangle)^2 \left(\frac{N}{\varepsilon_0 + \varepsilon_1 + N} \right)^{2k+2}.\end{aligned}\quad (52)$$

In the above expressions, for both even and odd poll indices k , $\text{Var}[A_\infty]$ stands for the stationary variance,

$$\text{Var}[A_\infty] = \frac{N\varepsilon_1\varepsilon_0(\varepsilon_0 + \varepsilon_1 + N)^2}{(\varepsilon_0 + \varepsilon_1)^2 [(\varepsilon_0 + \varepsilon_1)^2 + (2\varepsilon_0 + 2\varepsilon_1 + 1)N]}. \quad (53)$$

In Fig. 4 (c) we see that the analytical expressions for the evolution of variance matches the numerical simulations rather well.

While the stationary mean, Eq. (45), has a form identical to the mean of the Beta-binomial distribution, the stationary variance has a bit different form. Yet if the number of agents is large, $N \gg (\varepsilon_0 + \varepsilon_1)$, the difference in form becomes negligible. These results suggest that A_∞ could be well approximated by $\text{BetaBin}(N, 2\varepsilon_1, 2\varepsilon_0)$ distribution. This is confirmed by numerical simulation in Fig. 4 (d).